2022 American Control Conference (ACC)
Atlanta, USA, June 8-10, 2022

Robust Passively Safe Spacecraft Swarming via Closed-form and Optimization-based Control Approaches*

Tommaso Guffanti[1] and Simone D'Amico[2].

Abstract— **Miniaturized space-borne multi-agent systems, a.k.a spacecraft swarms, promise to overcome the limitations of monolithic satellites, across the board, from capabilities to mission costs. Nevertheless, the use of low-size-weight-and-power as well as commercial-off-the-shelf hardware make them more prone to contingencies which may cause loss of control capabilities. Therefore, spacecraft swarms shall be collision-free in the presence of contingencies that prevent trajectory re-planning and control on the short term. Passive safety consists in guaranteeing safe separation robust to control losses, while in presence of system uncertainties. This paper explores both closed-form and direct optimization-based approaches to swarm passive safety, highlighting advantages, limitations and comparing them on a representative test case drawn from the upcoming VIrtual Super Optics Reconfigurable Swarm (VISORS) mission. The underlying shared mathematical foundation is the modeling of the swarm dynamics through a state parameterization in integration constants. Such state choice provides unique geometrical intuition at closed-form level, and makes passive safety tractable at direct optimization level. In particular, it permits to exploit variation of parameters to reduce the number of constraints required to enforce passive safety, and to compensate for nonintegrable dynamics and uncertainty effects. Besides the key trades, this paper shows how the presented approaches can enable tight and reconfigurable satellite swarming in the presence of contingencies.**

I. INTRODUCTION

Multi-agent spaceborne systems demand high levels of safety, robustness and fault tolerance. Such risk-adversion is mainly dictated by the consequences a collision in space may have both in terms of debris generation and investment losses. In recent years, the trends of spacecraft bus miniaturization and use of low size-weight and power (low-SWaP) as well as commercial-of-the-shelf (COTS) hardware increased the likelihood of contingencies that directly or indirectly cause permanent or temporary incapability to control a spacecraft [1]. Fault tolerant strategies become therefore fundamental to mitigate the consequences and keep the risks associated to flying such systems within tolerable levels [2]. This paper focuses specifically on passive safety (PS), which consists in providing guarantees of safe separation robust to control losses, in presence of system uncertainties.

First attempts to account for PS into multi-agent control date back to the coelliptic rendevous of the Apollo missions [3], and lately to the colocation of geostationary satellites in shared longitude slots [4]. Subsequently, PS became a fundamental enabler of the first binary formation-flying missions in low earth orbit (LEO) [5]. Here, the relative orbits were designed such as safe separation was always guaranteed in the radial/normal orbital directions, irrespective of failures of controlling and/or estimating the separation in the along-track direction [6]. Idea then generalized to N-spacecraft swarms in near-circular orbits [7]. The main limitations of this literature are: 1) PS is explored at orbit design level and not as a formal constraint within the optimal control problem (OCP), 2) PS guarantees are given under assumptions on the orbit type and dynamics (e.g, near-circularity, linearized two-body dynamics, or with specific perturbations), 3) PS is enforced through possibly over-conservative constraints on the relative orbit design (e.g., energy matching conditions, sub-state designs). In general, these limitations cause the current state-of-the-art to fall short in addressing the needs required by future swarm missions, both in terms of applicability, breath and robustness.

Developing on preliminary works of the authors [8], [9], this paper contributes to the state-of-the-art by presenting a general mathematical framework to model swarm PS efficiently. This framework is based on the use of the integration constants (IC) of an integrable portion of the swarm dynamics as state variables. Using IC permits to leverage variation of parameters (VoP) [10] to achieve: 1) a reduction of the number of constraints required to enforce PS, 2) a compensation of nonintegrable dynamics and uncertainty effects. This motivates the use of closed-form analysis jointly with direct optimization to enforce PS efficiently within an OCP. In particular, the paper shows how direct optimization can generalize over closed-form analysis, while leveraging it to enforce PS in a tractable way. The result is a control algorithm that achieves passively safe spacecraft swarming efficiently in broader orbital scenarios, while in presence of realistic system uncertainties from sensing, actuation, and unmodeled system dynamics. In this paper, the direct optimization scheme used is based on sequential convex programming (SCP) [11], [12], and is combined with model predictive control (MPC) [13] to retrieve closed-loop properties.

The paper is structured as follows, Section II and III show how to model efficiently the swarm dynamics and PS using IC, Section IV develops improved closed-form expressions for swarm PS in eccentric orbits, Section V presents how to include PS efficiently within a generic OCP solvable through direct optimization, finally, Section VI compares the approaches on the upcoming VISORS mission [14].

*This work was supported by the VISORS's mission NSF Award #1936663. The authors are thankful for their support.

[1] Ph.D. Candidate, Aeronautics and Astronautics, Stanford University, Stanford, CA 94305, USA. tommaso@stanford.edu

[2] Associate Professor, Aeronautics and Astronautics, Stanford University, Stanford, CA 94305, USA. damicos@stanford.edu

II. SWARM DYNAMICS

The swarm motion in space is described by a reference orbit, either occupied by a chief spacecraft or virtual, and by N relative trajectories defined with respect to this reference. The reference orbit is uniquely defined by a set of orbital elements (OE): $\boldsymbol{\mathfrak{oe}} \in R^6$. Let us use the quasi non-singular OE definition [15]: $\boldsymbol{\mathfrak{oe}} = \{a, \lambda_\nu, e_x, e_y, i, \Omega\}$, with a the semi-major axis, $\lambda_\nu = \nu + \omega$ the true argument of latitude, ν the true anomaly, ω the argument of perigee, $\{e_x, e_y\} = \{e\cos(\omega), e\sin(\omega)\}$ the eccentricity vector, e the eccentricity, i the inclination, and Ω the right ascension of the ascending node. The N relative trajectories are defined by the relative Cartesian state expressed in the radial/along-track/normal (RTN) [15] frame centered on the reference, as $\boldsymbol{\chi}_k = \{\delta\boldsymbol{r}_k, \delta\dot{\boldsymbol{r}}_k\} \in R^6$, for $k = 1, \dots N$, where $\delta\boldsymbol{r}_k \in R^3$ and $\delta\dot{\boldsymbol{r}}_k \in R^3$ are correspondingly the relative position and velocity of the k^{th} spacecraft. The dynamics of $\boldsymbol{\chi}_k$ is governed by a set of nonlinear ODE [16]

$$\dot{\boldsymbol{\chi}}_k(t) = \boldsymbol{z}(\boldsymbol{\chi}_k(t)) + \boldsymbol{p}(\boldsymbol{\chi}_k(t)) + \boldsymbol{B}\boldsymbol{u}_k(t) \tag{1}$$

where, $\boldsymbol{z}(.) \in R^6$ models the relative effect of two-body spherical gravity as well as Euler, centrifugal and Coriolis accelerations raising from the non-inertial (and potentially perturbed) nature of the rotating RTN frame, $\boldsymbol{p}(.) \in R^6$ models the differential effect of orbital perturbations, and $\boldsymbol{u}_k \in R^3$ is the k^{th} spacecraft control acceleration expressed in RTN frame, with $\boldsymbol{B} = [\boldsymbol{0}_{3\times3}; \boldsymbol{I}_{3\times3}] \in R^{6\times3}$ the control input matrix. The relative dynamics in Eq. 1 depends on the reference OE, this dependence is let implicit in the notation for compactness. In literature, analytical solutions for the homogeneous nonlinear part of Eq. 1 are not available. Nevertheless, linearizing the differential spherical gravity terms in $\boldsymbol{z}(.)$ for small spacecraft separations, Eq. 1 is rewritten exactly as

$$\dot{\boldsymbol{\chi}}_k(t) = \boldsymbol{A}(t)\boldsymbol{\chi}_k(t) + \boldsymbol{d}(\boldsymbol{\chi}_k(t)) + \boldsymbol{B}\boldsymbol{u}_k(t) \tag{2}$$

where $\boldsymbol{A} \in R^{6\times6}$ is the linear(ized) integrable part, and $\boldsymbol{d}(.) \in R^6$ is the nonlinear nonintegrable part named hereafter the "disturbance term", which contains both $\boldsymbol{p}(.)$ and the truncated higher-order terms of $\boldsymbol{z}(.)$. Since the beginning of spaceflight, solutions for the linear part of Eq. 2 have been developed by different authors. For example, Hill, Clohessy and Wiltshire (HCW) developed a famous solution for spacecraft in near-circular orbits [17], whereas Yamanaka and Ankersen (YA) for spacecraft in eccentric orbits [18]. All these solutions share common structure: $\boldsymbol{\chi}_k(t) \approx \boldsymbol{\Psi}(t)\boldsymbol{c}_k$, where, $\boldsymbol{c}_k = \{c_{1,k}, c_{2,k}, c_{3,k}, c_{4,k}, c_{5,k}, c_{6,k}\} \in R^6$ is the k^{th} spacecraft IC state, and $\boldsymbol{\Psi}$ is the fundamental matrix solution of the linear ODE. Such fundamental matrix depends on time, usually through the true anomaly $\nu = \nu(t)$, but does not depend on the IC since the integrated ODE is linear. In this paper, the IC state selected is a tuned version of the YA's one. The associated $\boldsymbol{\Psi}$ is presented in Eq. 21 in Appendix as a function of the reference OE. $\boldsymbol{c}_k$ is non-dimensional, which makes the first three rows of $\boldsymbol{\Psi}$ having dimension of length, and the last three rows of length over time. $\boldsymbol{\Psi}$ models both bounded periodic motion and unbounded (unstable) motion. If $c_{1,k} \neq 0$, the motion is unstable in both along-track and radial direction if the reference orbit is eccentric, or just in along-track direction if the orbit is near-circular. If $c_{1,k} = 0$ the motion is bounded and periodic. In literature, the relative spacecraft state is modeled using relative orbital elements (ROE) as linear or nonlinear combination of the OE of two spacecraft or of a reference and a spacecraft. The ROE provide clear geometrical interpretation to the relative motion and are first-order equivalent of the IC [19]. Eq. 22 in Appendix provides a linear map between the used IC and the ROE. The effect of nonintegrable dynamics and control acceleration on the IC is modeled using VoP [10], as

$$\dot{\boldsymbol{c}}_k(t) = \boldsymbol{d}_c(t, \boldsymbol{c}_k(t)) + \boldsymbol{B}_c(t)\boldsymbol{u}_k(t) \tag{3}$$

where, the drift vector is $\boldsymbol{d}_c(t, \boldsymbol{c}_k(t)) = \boldsymbol{\Psi}^{-1}(t)\boldsymbol{d}(\boldsymbol{c}_k(t)) \in R^6$ and the control input matrix $\boldsymbol{B}_c(t) = \boldsymbol{\Psi}^{-1}(t)\boldsymbol{B} \in R^{6\times3}$.

Let us consider a closed-loop control setting where the swarm has to find a control plan $\tilde{\boldsymbol{u}}_k(t) \in R^3$, for $t \in [t_0, t_f]$, to move form an initial configuration at t_0 to a final one at t_f, acquiring at instants $t_e \in [t_0, t_f]$ an updated estimate of its IC state: $\tilde{\boldsymbol{c}}_k(t_e) \in R^6$. Such estimate is the mean of a Gaussian distribution: $\mathcal{N}(\tilde{\boldsymbol{c}}_k(t_e), \boldsymbol{C}_k(t_e))$, provided by the on-board navigation, where $\boldsymbol{C}_k(t_e) \in R^{6\times6}$ is the error covariance matrix. Let us assume the swarm has available on-board a model approximating the real disturbance term: $\tilde{\boldsymbol{d}}(.) \in R^3$. Using this model and VoP, the estimated mean state, $\tilde{\boldsymbol{c}}_k(t)$, is propagated for $t \geq t_e$, as

$$\dot{\tilde{\boldsymbol{c}}}_k(t) = \tilde{\boldsymbol{d}}_c(t, \tilde{\boldsymbol{c}}_k(t)) + \boldsymbol{B}_c(t)\tilde{\boldsymbol{u}}_k(t) \tag{4}$$

where, $\tilde{\boldsymbol{d}}_c(.) = \boldsymbol{\Psi}^{-1}(.)\tilde{\boldsymbol{d}}(.) \in R^6$. Moreoever, the covariance matrix, $\boldsymbol{C}_k(t)$, is propagated in a linearized sense as

$$\begin{aligned}\dot{\boldsymbol{C}}_k(t) =& \tilde{\boldsymbol{D}}_c(t, \tilde{\boldsymbol{c}}_k(t))\boldsymbol{C}_k(t) + \boldsymbol{C}_k(t)\tilde{\boldsymbol{D}}_c^T(t, \tilde{\boldsymbol{c}}_k(t)) \\ &+ \boldsymbol{B}_c(t)\boldsymbol{U}_k(t)\boldsymbol{B}_c^T(t) + \boldsymbol{Q}_k(t) + \boldsymbol{E}_k(t)\end{aligned} \tag{5}$$

where, $\tilde{\boldsymbol{D}}_c(.) = \frac{\partial\tilde{\boldsymbol{d}}_c(.)}{\partial\boldsymbol{c}}\big|_{\tilde{\boldsymbol{c}}_k} \in R^{6\times6}$. $\boldsymbol{U}_k(t) \in R^{3\times3}$ is the power spectral density of the zero-mean white Gaussian noise introduced by actuation on $\tilde{\boldsymbol{u}}(t)$. $\boldsymbol{Q}_k(t) \in R^{6\times6}$ is the power spectral density of the zero-mean white Gaussian process-noise capturing the difference: $\tilde{\boldsymbol{d}}_c(.) - \boldsymbol{d}_c(.)$. Finally, $\boldsymbol{E}_k(t) = \delta(t - t_{\tilde{e}})\boldsymbol{\mathcal{E}}(\boldsymbol{C}_k(t_{\tilde{e}})) \in R^{6\times6}$ models the effect of expected future measurements on the covariance, where $\delta(.)$ is the Dirac delta function, and $\boldsymbol{\mathcal{E}}(.)$ is a function of the predicted estimated covariance at future measurement instant $t_{\tilde{e}}$. Modeling the effect of future measurements informs intermediate open-loop control solutions of the closed-loop covariance behavior, preventing possible unfeasibility due to the growth of the uncertainty propagated in open-loop.

III. SWARM PASSIVE SAFETY

PS consists in providing guarantees of safe separation robust to control losses, in presence of system uncertainties. Different classes can be considered, depending on the type of contingency causing the control loss and the number of spacecraft involved. In this paper, PS has to guarantee separation $\geq \epsilon \in R_{>0}$ even if any subset or combination of

spacecraft lose control at any instant in $(t_0, t_f]$, without being able to recover it and re-plan to avoid collision until $t_f + T$. This in presence of uncertainties from navigation, actuation, and process-noise. Fig. 1 gives a graphical representation. The challenges in guaranteeing such level of safety are: 1) the

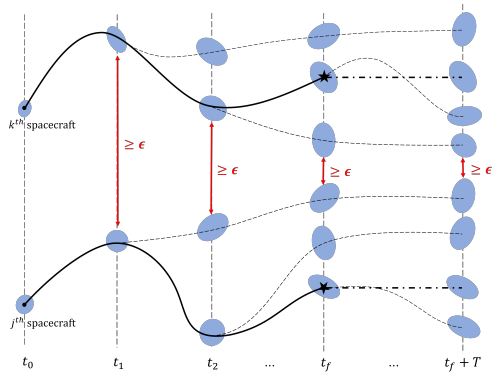

Fig. 1. Passive safety (PS). The spacecraft controlled trajectories are in solid lines, the uncontrolled ones in dashed lines, the shaded blue ellipses represent the uncertainty distributions of the Cartesian position evaluated at q-σ confidence interval.

dynamics governing the motion after a contingency is generally nonintegrable in closed-form, 2) the minimum separation between spacecraft has to be computed over the uncertainty distributions evaluated at a specified q-σ confidence interval, where $q \in N_{>0}$ and σ is a statistical standard deviation, 3) in a discrete-time setting, the number of constraints is polynomial (super-linear) in the number of discrete time samples in $(t_0, t_f + T]$ [9]. Nevertheless, the use of IC as state variables enables to exploit VoP, and specifically, a geometrical interpretation of VoP known as the "osculation principle" (OP) [15], presented in Fig. 2. OP states that the trajectory followed by one spacecraft in Cartesian space under action of integrable dynamics, disturbance term and control (Eq. 2), is instantaneously tangent to the manifold of the integrated dynamics associated to the value the IC state assumes at that instant through Eq. 3. Let us use OP

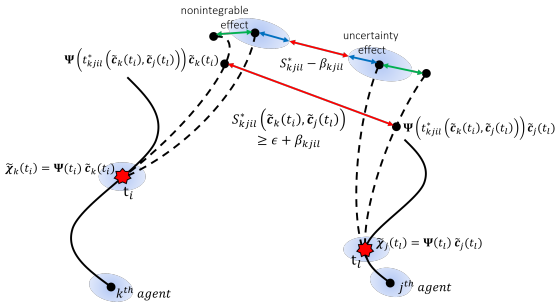

Fig. 2. Osculation principle (OP) and PS modeling. The motion of $\boldsymbol{\chi}(t)$ governed by Eq. 2 is instantaneously contained in $\boldsymbol{\Psi}(t)\boldsymbol{c}(t)$, with the evolution in time of $\boldsymbol{c}(t)$ governed by Eq. 3. The bound β_{kjil} accounts for effects of nonintegrable dynamics and uncertainties on the minimum separation $\mathcal{S}^*_{kjil}$ between agents k^{th} and j^{th} who loss control at instants t_i and t_l respectively.

to model PS. In particular, let us assume that, at instant t_i, a contingency affects spacecraft k^{th} which is not capable to control anymore $\forall t \in [t_i, t_f + T]$. According to OP, if at instant t_i the disturbance term is turned off too, the spacecraft starts moving on the manifold of the integrated dynamics defined as: $\boldsymbol{\Psi}(t)\boldsymbol{c}_k(t_i)$, $\forall t \in [t_i, t_f + T]$. Where $\boldsymbol{c}_k(t_i)$ is obtained integrating Eq. 3 up to t_i. Similarly, it can be said for any other j^{th} spacecraft which may lose control at instant t_l. Therefore, assuming the dynamics after contingency integrable, the PS constraint for the couple kj is written as

$$\mathcal{S}_{kjil}(t) = ||\boldsymbol{S}\boldsymbol{\Psi}(t)\left(\boldsymbol{c}_k(t_i) - \boldsymbol{c}_j(t_l)\right)||_2 \geq \epsilon \tag{6}$$

$\forall t_i \in (t_0, t_f]$, $\forall t_l \in (t_0, t_f]$, $\forall t \in [\max\{t_i, t_l\}, t_f + T]$; for $k = 1, \ldots N-1$, $j = k+1, \ldots N$. Where $\boldsymbol{S} \in R^{3\times 6}$ selects the relevant components within the state, and $||.||_2$ is the 2-norm. For example, if safe separation is enforced in 3-D then $\boldsymbol{S} = [\boldsymbol{I}_{3\times 3}, \boldsymbol{0}_{3\times 3}]$, if in RN plane then the left-block's diagonal is $[1, 0, 1]$, if in RT plane then it is $[1, 1, 0]$. A necessary and sufficient condition of Eq. 6 is

$$\mathcal{S}^*_{kjil} = \mathcal{S}_{kjil}(t^*_{kjil}) = ||\boldsymbol{S}\boldsymbol{\Psi}(t^*_{kjil})\left(\boldsymbol{c}_k(t_i) - \boldsymbol{c}_j(t_l)\right)||_2 \geq \epsilon \tag{7}$$

with

$$t^*_{kjil} = \arg \min_{t\in[\max\{t_i,t_l\},t_f+T]} \{\mathcal{S}_{kjil}(t)\} \tag{8}$$

$\forall t_i \in (t_0, t_f]$, $\forall t_l \in (t_0, t_f]$, for $k = 1, \ldots N-1$, $j = k+1, \ldots N$. Where, t^*_{kjil} is the instant at which agents k^{th} and j^{th} reach minimum separation on the uncontrolled trajectories generated by control losses at instant t_i and t_l respectively, and $\mathcal{S}^*_{kjil}$ is such minimum separation. Note that, by using OP (Eq. 6), $\mathcal{S}_{kjil}(t)$ is a closed-form expression of the IC. Therefore, t^*_{kjil} results being a function of $\boldsymbol{c}_k(t_i)$ and $\boldsymbol{c}_j(t_l)$. This makes $\mathcal{S}^*_{kjil}$ a function of the IC states and independent from the time along the uncontrolled trajectories, as

$$\mathcal{S}^*_{kjil} = \mathcal{S}^*_{kjil}(\boldsymbol{c}_k(t_i), \boldsymbol{c}_j(t_l)) \tag{9}$$

This has an important implication:

Remark III.1. *Assuming that the dynamics is integrable after a contingency, safe separation all-along the uncontrolled trajectories is enforced through a constraint on the IC states evaluated at the contingency instants, which is independent from the time along the uncontrolled trajectories.*

Remark III.1 directly implies that, to enforce PS, safe separation does not have to be checked at each instant along the uncontrolled arcs but just once per $kjil$-combination using Eq. 7-8. This reduces the number of constraints required to enforce PS by one polynomial degree of the number of discrete time samples [9]. Specifically, from cubic to quadratic for each couple of active agents, or from quadratic to linear if one agent in the couple is permanently passive (as for the VISORS mission scenario in Section VI).

Nevertheless, the effects on $\mathcal{S}^*_{kjil}$ of nonintegrable dynamics and uncertainties need to be accounted for. To that end, the net effect due to uncertainty on the state along the controlled trajectory at instant t_i is quantified as

$${}_{\sigma}\boldsymbol{\Delta}_{ki} = \left| \frac{\partial \mathcal{S}^*_{kjil}}{\partial \boldsymbol{c}_k}\bigg|_{\tilde{\boldsymbol{c}}_k(t_i)} q\sqrt{Diag(\boldsymbol{C}_k(t_i))} \right| \tag{10}$$

where, ${}_{\sigma}\boldsymbol{\Delta}_{ki} \in R_{\geq 0}$, $\partial \mathcal{S}^*/\partial \boldsymbol{c} \in R^s$, and the $Diag(.)$ operator extracts the diagonal vector from a square matrix. Moreover Eq. 4-5 are used to quantify the integrated effect due to nonintegrable dynamics on the estimated mean state and covariance along the uncontrolled trajectories over $[t_i, t_i + T]$, as

$$
\begin{aligned}
{}_{d}\boldsymbol{\Delta}_{ki} = & \left| \frac{\partial \mathcal{S}^*_{kjil}}{\partial \boldsymbol{c}_k} \right|_{\tilde{\boldsymbol{c}}_k(t_i)} \int_{t_i}^{t_f+T} \tilde{\boldsymbol{d}}_c(\tau, \tilde{\boldsymbol{c}}_k(\tau)) d\tau \Bigg| \\
& + \left| \frac{\partial \mathcal{S}^*_{kjil}}{\partial \boldsymbol{c}_k} \right|_{\tilde{\boldsymbol{c}}_k(t_i)} q \sqrt{\left| Diag\left(\int_{t_i}^{t_f+T} \tilde{\boldsymbol{D}}_c(\tau, \tilde{\boldsymbol{c}}_k(\tau)) \boldsymbol{C}_k(\tau) + \boldsymbol{C}_k(\tau) \tilde{\boldsymbol{D}}_c^T(\tau, \tilde{\boldsymbol{c}}_k(\tau)) + \boldsymbol{Q}_k(\tau) d\tau \right) \right|}
\end{aligned}
\tag{11}
$$

where, ${}_{d}\boldsymbol{\Delta}_{ki} \in R_{\geq 0}$, and the absolute value $|.|$ is applied element-wise for vector quantities. Note that $\tilde{\boldsymbol{c}}_k(t_i)$ and $\boldsymbol{C}_k(t_i)$ are obtained by propagating Eq. 4-5 up to contingency instant t_i. This is done identically for the j^{th} spacecraft. Let assume these effects are bounded, as

$$
{}_{\sigma}\boldsymbol{\Delta}_{ki} + {}_{d}\boldsymbol{\Delta}_{ki} + {}_{\sigma}\boldsymbol{\Delta}_{jl} + {}_{d}\boldsymbol{\Delta}_{jl} \leq \beta_{kjil} \tag{12}
$$

where $\beta_{kjil} \in R_{\geq 0}$ is a bounding constant. Using this bound, a sufficient condition of PS, robust to nonintegrable dynamics and q-σ uncertainty, is

$$
\mathcal{S}^*_{kjil}(\tilde{\boldsymbol{c}}_k(t_i), \tilde{\boldsymbol{c}}_j(t_l)) \geq \epsilon + \beta_{kjil} \tag{13}
$$

$\forall t_i \in (t_0, t_f]$, $\forall t_l \in (t_0, t_f]$, for $k = 1, \dots N-1$, $j = k+1, \dots N$. Here, $\mathcal{S}^*_{kjil}$ is evaluated at the estimated mean IC state values. Note how this sufficient condition entails the reduced number of constraints implied by Remark III.1. A graphical representation is provided in Fig. 2. In the following of the paper for compactness: $\epsilon_{kjil} = \epsilon + \beta_{kjil}$.

IV. CLOSED-FORM ANALYSIS

Closed-form analysis aims to provide an analytical expression to $\mathcal{S}^*_{kjil}$, or to a lowerbound $\underline{\mathcal{S}}^*_{kjil} \leq \mathcal{S}^*_{kjil}$. To that end, Eq. 7-8 have to be solved analytically using $\boldsymbol{\Psi}$ in Eq. 21 in Appendix. The full 3-D solution for swarm in eccentric orbit accounting for both bounded and unbounded motion is rather complicated. Therefore in literature [6], [7], authors have developed reduced solutions by: 1) assuming $c_{1,k} \sim 0$, $\forall k$, and so enforcing the relative motion bounded and periodic for all spacecraft, 2) decomposing the full 3-D problem in two 2-D sub-problems (RN and RT), 3) assuming near-circular orbits. In this section, the third assumption is removed, and two lowerbounds: $\underline{\mathcal{S}}^{*RN}_{kjil}$ and $\underline{\mathcal{S}}^{*RT}_{kjil}$, are computed for swarm in eccentric orbits. Here, the superscripts RN/RT refer to the sub-planes in which the minimum separation is computed. To that end, for compactness, let us define: $\boldsymbol{c}_{kjil} = \boldsymbol{c}_k(t_i) - \boldsymbol{c}_j(t_l)$. Using this notation and assuming $c_{1,k} \sim 0$, from Eq. 21, the first three components of $\boldsymbol{\Psi}(t)\boldsymbol{c}_{kjil}$ are

$$
\begin{aligned}
\delta r_{R,kjil}(t) &\approx -a c_{34,kjil} \cos(\lambda_\nu(t) - \theta_{34,kjil}) \\
\delta r_{T,kjil}(t) &\approx \frac{1}{\rho(\nu(t))} a c_{2,kjil} + \Big(\frac{1}{\rho(\nu(t))} + 1\Big) a c_{34,kjil} \sin(\lambda_\nu(t) - \theta_{34,kjil}) \\
\delta r_{N,kjil}(t) &\approx \frac{1}{\rho(\nu(t))} a c_{56,kjil} \sin(\lambda_\nu(t) - \theta_{56,kjil})
\end{aligned}
\tag{14}
$$

which represent the relative position of k^{th} and j^{th} spacecraft along the uncontrolled trajectories generated by control losses at instant t_i and t_l respectively. The IC state has been expressed in polar form $\boldsymbol{c}_{ab,kjil} = \{c_{a,kjil}, c_{b,kjil}\} = c_{ab,kjil}\{\cos(\theta_{ab,kjil}), \sin(\theta_{ab,kjil})\}$. In Eq. 14, the terms function of $\rho(\nu(t))$ hinder a clear geometrical interpretation of the motion. In particular, $\rho(\nu) = 1 + e\cos(\nu) \in [1-e, 1+e]$. Its two extreme values are achieved at the apogee and at the perigee of the eccentric orbit. If $\rho(\nu)$ is fixed to $\bar{\rho} \in [1-e, 1+e]$, Eq. 14 has geometrical representation as in Fig. 3. Such representation is not the real relative

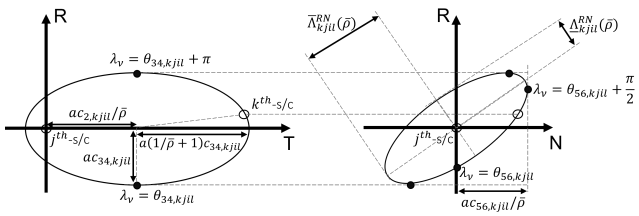

Fig. 3. Geometrical representation of Eq. 14, fixing $\rho(\nu(t)) = \bar{\rho}$. In near-circular orbit, being $\rho(\nu(t)) \approx 1\ \forall t$, it becomes the true representation of the relative motion.

motion in eccentric orbit, which includes $\rho(\nu)$ as a time varying function of the true anomaly. On the other hand, at each $\nu(t) = \bar{\nu}$, the real relative motion trajectory is tangent to the ellipses in Fig. 3 at the point $\lambda_\nu = \omega + \bar{\nu}$, with $\bar{\rho} = 1 + e\cos(\bar{\nu})$. This implies that, a lowerbound of the real separation between spacecraft on the uncontrolled trajectories can be computed in either RN or RT planes by evaluating the minimum separations of the two ellipses from the origin. As presented in the following, these minimum separations assume extremal values at the perigee and apogee of the eccentric orbit. The minima of these extremals are by definition lowerbounds of $\mathcal{S}^*_{kjil}$, and can be used in Eq. 13 to achieve PS. Being the uncontrolled relative motion assumed bounded and periodic, PS is achieved infinitely (T=∞). Nevertheless, assuming $c_{1,k} \sim 0$ can be rather limiting, and is overcome by direct optimization in Section V.

A. Passive Safety in RN-plane

The minimum separation of the RN ellipse from the origin is computed as the minimum eigenvalue $\underline{\Lambda}^{RN}_{kjil}(\bar{\rho})$ of a singular value decomposition (Fig. 3, right) as

$$
\underline{\mathcal{S}}^{*RN}_{kjil}(\bar{\rho}) = \frac{\sqrt{2} a |\boldsymbol{c}_{34,kjil} \cdot \frac{\boldsymbol{c}_{56,kjil}}{\bar{\rho}}|}{\left[(c_{34,kjil})^2 + \left(\frac{c_{56,kjil}}{\bar{\rho}} \right)^2 + |\boldsymbol{c}_{34,kjil} + \frac{\boldsymbol{c}_{56,kjil}}{\bar{\rho}}| \cdot |\boldsymbol{c}_{34,kjil} - \frac{\boldsymbol{c}_{56,kjil}}{\bar{\rho}}| \right]^{1/2}} \tag{15}
$$

Consistently with Remark III.1, $\underline{\mathcal{S}}^{*RN}_{kjil}(\bar{\rho})$ is, for a fixed value of $\bar{\rho}$, independent from time and function of the IC states evaluated at the contingency instants. Taking the partials with respect to $\bar{\nu}$, its smallest and largest values are achieved correspondingly at the perigee and apogee of the eccentric orbit. Therefore, a lowerbound over the full orbit is obtained substituting $\bar{\rho}$ with $1+e$. Using Eq. 15, the sufficient condition of PS in Eq. 13 can be rewritten as

$$
|\hat{\boldsymbol{c}}_{34,kjil} \cdot \hat{\boldsymbol{c}}_{56,kjil}| = |\cos(\theta_{34,kjil} - \theta_{56,kjil})| \geq \cos(\xi_{kjil}(\bar{\rho})) \tag{16}
$$

with

$$
\cos(\xi_{kjil}(\bar{\rho})) = \frac{\epsilon_{kjil}\bar{\rho}}{a c_{34,kjil} c_{56,kjil}} \sqrt{(c_{34,kjil})^2 + \left(\frac{c_{56,kjil}}{\bar{\rho}} \right)^2 - \frac{\epsilon^2_{kjil}}{a^2}} \tag{17}
$$

$\forall t_i \in (t_0, t_f]$, $\forall t_l \in (t_0, t_f]$, for $k = 1, \dots N-1$, $j = k+1, \dots N$. Where, $\boldsymbol{c}_{ab,kjil} = c_{ab,kjil}\hat{\boldsymbol{c}}_{ab,kjil}$. Eq. 16-17 have an interesting geometrical interpretation in IC space, as presented in Fig. 4. In particular, to maintain PS in RN-plane the phase angle between the vectors $\boldsymbol{c}_{34,kjil}$ and $\boldsymbol{c}_{56,kjil}$, i.e. $\theta_{34,kjil} - \theta_{56,kjil}$, must be either contained in the interval $[-\xi_{kjil}(\bar{\rho}),\ \xi_{kjil}(\bar{\rho})]$ (parallel configuration) or in the interval $[\pi - \xi_{kjil}(\bar{\rho}),\ \pi + \xi_{kjil}(\bar{\rho})]$ (anti-parallel configuration), where the most and least tight conditions are achieved correspondingly at the perigee and apogee of the eccentric orbit. Eq. 16-17 represent the $\boldsymbol{c}_{34}/\boldsymbol{c}_{56}$-separation concept, which in near-circular orbit, using ROE, becomes the relative eccentricity/inclination-separation concept [6], flown in LEO [5].

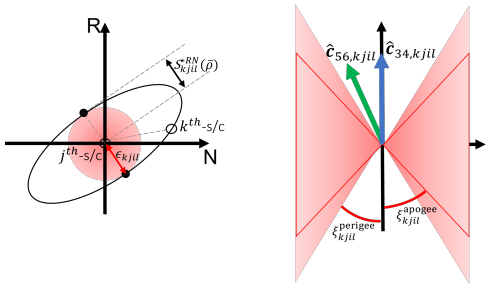

Fig. 4. Graphical representation of the sufficient condition of RN-passive safety in Cartesian space (on the left) and in IC space (on the right), for swarms in eccentric orbits.

B. Passive Safety in RT-plane

The minimum separation of the RT ellipse from the origin is computed solving analytically Eq. 8 as a function of λ_ν, by using Eq. 14 and fixing $\bar{\rho}$. This results in a minimum separation of

$$\underline{\mathcal{S}}^{*RT}_{kjil}(\bar{\rho}) \begin{cases} = a\frac{1}{\bar{\rho}}c_{2,kjil} - a\left(\frac{1}{\bar{\rho}}+1\right)c_{34,kjil} & \text{not-encircling} \\ = \begin{cases} \sqrt{a^2c^2_{34,kjil} - \frac{1}{1+2\bar{\rho}}a^2c^2_{2,kjil}} & \frac{\epsilon_{kjil}}{a} \le c_{34,kjil} < \frac{1+\bar{\rho}}{\bar{\rho}}\frac{\epsilon_{kjil}}{a} \\ a\left(\frac{1}{\bar{\rho}}+1\right)c_{34,kjil} - a\frac{1}{\bar{\rho}}c_{2,kjil} & c_{34,kjil} \ge \frac{1+\bar{\rho}}{\bar{\rho}}\frac{\epsilon_{kjil}}{a} \end{cases} & \text{encircling} \end{cases} \tag{18}$$

where "not-encircling" refers to Fig. 5, top left, whereas, "encircling" refers to Fig. 5, center and bottom left. Consistently with Remark III.1, $\underline{\mathcal{S}}^{*RT}_{kjil}(\bar{\rho})$ is, for a fixed value of $\bar{\rho}$, independent from time and function of the IC states evaluated at the contingency instants. Taking the partials with respect to $\bar{\nu}$, its smallest and largest values are achieved correspondingly at the perigee and apogee of the eccentric orbit for the not-encircling case, and at the apogee and perigee for the encircling case. Therefore, a lowerbound over the full orbit can be obtained by substituting $\bar{\rho}$ with $1+e$ for the not-encircling case, whereas with $1-e$ for the encircling case. Using Eq. 18, the sufficient condition of PS in Eq. 13 can be rewritten as

$$|c_{2,kjil}| \begin{cases} \ge (1+\bar{\rho})c_{34,kjil} + \frac{\epsilon_{kjil}}{a} & \text{not-encircling} \\ \le \begin{cases} \sqrt{(1+2\bar{\rho})(c^2_{34,kjil} - \frac{\epsilon^2_{kjil}}{a^2})} & \text{if } \frac{\epsilon_{kjil}}{a} \le c_{34,kjil} < \frac{1+\bar{\rho}}{\bar{\rho}}\frac{\epsilon_{kjil}}{a} \\ (1+\bar{\rho})c_{34,kjil} - \frac{\epsilon_{kjil}}{a} & \text{if } c_{34,kjil} \ge \frac{1+\bar{\rho}}{\bar{\rho}}\frac{\epsilon_{kjil}}{a} \end{cases} & \text{encircling} \end{cases} \tag{19}$$

$\forall t_i \in (t_0, t_f]$, $\forall t_l \in (t_0, t_f]$, for $k = 1, \dots N-1$, $j = k+1, \dots N$. In IC space, Eq. 19 has representation as in Fig. 5, right, where the most tight and least tight conditions are achieved correspondingly at the perigee and apogee for the not-encircling case, and at the apogee and perigee for the encircling case. In near-circular orbit, using ROE, Eq. 19 reduces to the solutions in [7].

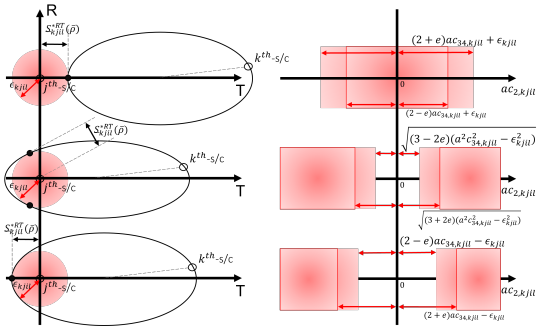

Fig. 5. Graphical representation of the sufficient condition of RT-passive safety in Cartesian space (on the left) and in IC space (on the right), for swarms in eccentric orbits.

V. DIRECT OPTIMIZATION

Closed-form analysis provides clear geometrical intuition to PS, which can be leveraged for swarm orbit design and guidance. Nevertheless, it is limited by the assumptions introduced, which can be over-constraining in scenarios where PS has to be achieved without enforcing boundedness or has not to be restricted to a 2-D sub-plane. The direct optimization approach aims to include directly Eq. 13 within an OCP, accounting for the full $\boldsymbol{\Psi}$ (as in Eq. 21 in Appendix) and taking $\boldsymbol{S}$ as an input parameter to select the desired PS class (e.g., 3-D, RN or RT). Specifically, in closed-loop [13], the OCP the swarm must solve, possibly at every instant $t_e \in [t_0, t_f]$ an updated state estimate is available, until a specified target set $\boldsymbol{\mathcal{C}}_{k,f}$ is reached at t_f, is

Problem V.1.

$$\begin{aligned} \underset{\tilde{\boldsymbol{u}}_k(t)}{\text{minimize}} \quad & \sum_{k=1}^{N}\int_{t_e}^{t_f} \mathcal{J}(\tilde{\boldsymbol{c}}_k(t), \boldsymbol{C}_k(t), \tilde{\boldsymbol{u}}_k(t), t)dt \\ \text{subject to} \quad & \dot{\tilde{\boldsymbol{c}}}_k(t) = \tilde{\boldsymbol{d}}_c(t, \tilde{\boldsymbol{c}}_k(t)) + \boldsymbol{B}_c(t)\tilde{\boldsymbol{u}}_k(t) && \forall t \in [t_e, t_f],\ k = 1, \dots N \\ & \dot{\boldsymbol{C}}_k(t) = \tilde{\boldsymbol{D}}_c(t, \tilde{\boldsymbol{c}}_k(t))\boldsymbol{C}_k(t) + \boldsymbol{C}_k(t)\tilde{\boldsymbol{D}}^T_c(t, \tilde{\boldsymbol{c}}_k(t)) && \forall t \in [t_e, t_f],\ k = 1, \dots N \\ & \qquad + \boldsymbol{B}_c(t)\boldsymbol{U}_k(t)\boldsymbol{B}^T_c(t) + \boldsymbol{Q}_k(t) + \boldsymbol{E}_k(t) \\ & \mathcal{S}^*_{kjil}(\tilde{\boldsymbol{c}}_k(t_i), \tilde{\boldsymbol{c}}_j(t_l)) \ge \epsilon_{kjil} && \forall t_i \in (t_e, t_f],\ \forall t_l \in (t_e, t_f], \\ & && k = 1, \dots N-1,\ j = k+1, \dots N \\ & \tilde{\boldsymbol{u}}_k(t) \in \boldsymbol{\mathcal{U}}_k && \forall t \in [t_e, t_f],\ k = 1, \dots N \\ & \mathcal{N}(\tilde{\boldsymbol{c}}_k(t_f), \boldsymbol{C}_k(t_f)) \in \boldsymbol{\mathcal{C}}_{k,f} && k = 1, \dots N \\ & \mathcal{N}(\tilde{\boldsymbol{c}}_k(t_e), \boldsymbol{C}_k(t_e)) \equiv \textit{ state estimate} && k = 1, \dots N \end{aligned} \tag{20}$$

Where, $\mathcal{J}(.) \in R_{>0}$ is a generic cost functional modeling control input and/or time minimization as well as other factors, and $\boldsymbol{\mathcal{U}}_k$ is the set of admissible control inputs. Problem V.1 enforces PS for at least T of at least ϵ at q-σ confidence over $(t_e, t_f]$. The PS constraint requires the evaluation of Eq. 7-8 as well as the quantification of the bound through Eq. 10-12. The authors presented in [9] a solution approach based on SCP. From an algorithmic perspective, the turning point lies in the availability or not of an analytical expression for $\mathcal{S}^*_{kjil}(\tilde{\boldsymbol{c}}_k(t_i), \tilde{\boldsymbol{c}}_j(t_l))$ (or a lowerbound). If an analytical expression is available, then $\mathcal{S}^*_{kjil}$ is sequentially linearized within the SCP framework, being in general not convex. If an analytical expression is not available, due to the fact that Eq. 8 may be rather complicated to be solved in closed-form,

then an algorithmic development is needed. In particular, at each iteration of the SCP loop, t^*_{kjil} is precomputed at the current SCP reference using a simple search algorithm on the discretized interval $[\max\{t_i, t_l\}, t_f + T]$. This search algorithm selects the instant/index that minimizes $\mathcal{S}_{kjil}(t)$, available in closed-form using OP (Eq. 6). Then, $\mathcal{S}_{kjil}(t)$ is evaluated at this instant/index within Problem V.1, permitting to enforce PS through the reduced number of constraints implied by Remark III.1. t^*_{kjil} is sequentially updated within the SCP pipeline to guarantee that, at convergence, the actual minimum separation is greater then ϵ_{kjil}. In both cases, using IC permits to enforce PS through the reduced number of constraints, cut the computational expense, and increase the chances of converging in useful time to a feasible solution using off-the-shelf solvers [20], [21].

VI. NUMERICAL RESULTS

VISORS is a two 6U CubeSats distributed telescope that will operate in a near-circular sun-synchronous LEO to image coronal area of the sun with unprecedented resolution [14]. One spacecraft (OSC) contains the optical payload, the other (DSC) contains the detector. During nominal operations, DSC acts as passive chief, whose center of mass sets the RTN frame's origin, whereas OSC actively controls the relative motion. The test case considered models the challenging "transfer phase", where a passively safe control plan that moves the swarm from the stand-by mode (initial condition) to the science mode (final condition) has to be computed. Both modes are designed in closed-form to achieve PS in RN plane through relative eccentricity/inclination-separation [6]. Nevertheless, PS has not only to be guaranteed at initial and terminal states, but at every instant of the transfer too. Therefore, direct optimization has to be leveraged to generalize over pure closed-form analysis and compute the transfer. All the parameters of the reconfiguration scenario are reported in Table I-II. It is a two orbits transfer, in which the 2-norm of the control input is minimized, and PS is guaranteed in RN plane for at least two orbits (T), of at least 3m (ϵ), at 3-σ confidence (q). The uncertainty stems from differential GPS navigation [22], cold-gas impulsive actuation [23] and process-noise modeling the discrepancy between the full-force ground-truth [14], [22] and the on-board dynamics model [24], [25], [26].

At each SCP iteration, an instance of Problem V.1 is solved as a second order cone program (SOCP) [20]. The optimizer looks for candidate maneuvers every 30deg, so the interval $[t_0, t_f]$ is discretized in 25 samples. PS is enforced after each maneuver application. This guarantees safety both on the trajectory in between maneuvers and, in case of subsequent maneuver failure, afterwards up to $t_f + T$. The intervals $[t_i, t_f + T]$, over which t^*_{kjil} is precomputed, are discretized at 1deg, so ≥ 721 samples depending on t_i. The proposed efficient $\mathcal{S}^*_{kjil}$ formulation permits to reduce the number of constraints required to enforce PS from $> 25 \times 721 = 18025$ to 25. By explicitly enforcing these constraints within the SOCP, this implies in average a computational saving of a factor > 100 (from $\sim 90s$ to $\sim 0.55s$) on the solution of an instance of Problem V.1 using a SOCP solver [21] on a computer equipped with a 1.8GHz processor and 8GB RAM. The computational overhead introduced by the precomputation of t^*_{kjil} is minimal, since it is performed jointly with the precomputations required to evaluate β_{kjil} as well as other matrices needed in the SOCP, for a total time $\sim 4s$. Note that, if all the thousands constraints are enforced explicitly and t^*_{kjil} is not computed, precomputations are still needed at each SCP iteration but may be slightly lighter (few seconds gain, depending on the implementation). On the other hand, the computational gain obtained on the solution of the SOCP by enforcing just 25 constraints is much greater.

Numerical results are presented in Fig. 6 and 7. Looking at Fig. 6, the 3-D RTN trajectory of the OSC around the DSC (at the origin) is presented on the left, whereas its 2-D RN projection is presented on the right. Direct optimization provides a passively safe reconfiguration between standby and science modes. In particular, the controlled motion (blue bold line) is always instantaneously tangent to a safe uncontrolled trajectory (dashed lines), which is followed if the OSC loses control at that instant. Spacecraft separation along the uncontrolled trajectories is guaranteed to be $\geq$ 3m for at least 2 orbits, accounting for 3-σ uncertainty (blue shaded ellipsoids). This is achieved in closed-loop. At t_0, a first navigation solution is acquired and Problem V.1 is solved for an open-loop control profile up to instant t_f. Then at each subsequent t_e, a new navigation solution is acquired and Problem V.1 is solved again for an updated control plan. The black dot-dashed "closed-loop plan" line is the trajectory planned on-board. The blue "controlled true" line is obtained by executing the control plan through actuation and propagating the resulting motion through the ground-truth dynamics. The difference between these two lines lies in the difference between the on-board dynamics model and the ground-truth, as well as in the errors introduced by navigation and actuation. Similar can be said for the dashed "uncontrolled" trajectories. The blue ones are obtained integrating the ground-truth dynamics after each possible contingency. The black ones are predicted on-board and have superimposed the 3-σ ellipsoids modeling the uncertainty distributions used to compute the bounds β_{kjil}. The true uncontrolled trajectories are contained within the 3-σ ellipsoids implying that the uncertainty distributions rightly capture and compensate for the difference between on-board belief and reality. Note how larger uncertainty manifests after larger maneuvers application, due to the correlation between maneuver magnitude and actuation uncertainty presented in Table I. The total control cost of the transfer is 0.27m/s. The cost of the unconstrained two-point-boundary-value-problem is $\sim$0.253m/s. A difference of 10%, considering the included constraints and uncertainties, represents a very fuel efficient transfer, well within the $\sim$0.3m/s allocated in the mission delta-V budget [14]. Finally, to compare with closed-form analysis, Fig. 7 shows the evolution over the transfer of $a\boldsymbol{c}_1$ (left), the magnitude of the vectors $a\boldsymbol{c}_{34}$/$a\boldsymbol{c}_{56}$ (center), and their angular separation (right). The magnitude of $\boldsymbol{c}_{34}$ and $\boldsymbol{c}_{56}$ sizes the ellipses drawn by uncontrolled trajectories in

RN plane (see Fig. 3, right), whereas, $\boldsymbol{c}_1$ represents an off-set in radial direction of these ellipses (see Eq. 21, in Appendix). The trajectory computed using direct optimization achieves PS in RN plane either by having these ellipses centered around the origin with size $\geq \epsilon_{kjil}$, or, by decentering them in radial direction through a sufficiently large $|\boldsymbol{c}_1|$ if their size is $< \epsilon_{kjil}$ (see Fig. 6, right). This analysis is validated in Fig. 7. At the second maneuver, the reduction of the $\boldsymbol{c}_{34}$ and $\boldsymbol{c}_{56}$ norms requires $\boldsymbol{c}_1 \approx -80$m to achieve PS in RN plane. Looking at the $\boldsymbol{c}_{34}$/$\boldsymbol{c}_{56}$-separation, when the norm of $\boldsymbol{c}_{34}$ or $\boldsymbol{c}_{56}$ becomes $< \epsilon_{kjil}$, ξ_{kjil} (Eq. 17) shrinks so much that safe separation is not possible by centering the RN ellipse around the origin. Therefore PS is achieved by properly decentering the ellipse in radial direction. The notable aspect is that such clear geometrical insight and deep connection with closed-form analysis is obtained solving Problem V.1 through direct optimization. This opens the way to much greater generalization and applicability reach than the specialized closed-form solutions.

VII. CONCLUSIONS

Fault tolerant strategies such as passive safety (PS) are important in risk-adverse and failure-sensitive applications as miniaturized spacecraft swarming, employing low size-weight and power as well as commercial-of-the-shelf components. Specifically, PS consists in providing guarantees of safe separation robust to control losses, in presence of system uncertainties. In this paper, a general mathematical approach based on the use of the integration constants (IC) of an integrable portion of the governing dynamics as state variables is proposed to model PS efficiently. In particular, IC permit to exploit variation of parameters to reduce the number of constraints needed to enforce PS, and to compensate for nonintegrable dynamics and uncertainties. Based on this approach both closed-form analysis and direct optimization are leveraged to improve over the state-of-the-art in passively safe swarm control. In particular, direct optimization can generalize upon closed-form analysis, but on the other hand, it has to be informed by closed-form analysis to enforce PS in a tractable and efficient way for on-board execution.

APPENDIX

The fundamental matrix solution of the linear(ized) integrable part of Eq. 2 is

$$\boldsymbol{\Psi}(t) = a \left[\begin{array}{c|c|cc|cc} \frac{1}{\rho} - \frac{3}{2}\frac{e}{\eta^3}\sin(\nu)nt & 0 & -\cos(\lambda_\nu) & -\sin(\lambda_\nu) & 0 & 0 \\ -\frac{3}{2}\frac{M}{\eta^3}nt & \frac{1}{\rho} & (\frac{1}{\rho}+1)\sin(\lambda_\nu) & -(\frac{1}{\rho}+1)\cos(\lambda_\nu) & 0 & 0 \\ 0 & 0 & 0 & 0 & \frac{1}{\rho}\sin(\lambda_\nu) & -\frac{1}{\rho}\cos(\lambda_\nu) \\ -\frac{1}{\rho^2}\dot{\rho} - \frac{3}{2}\frac{e}{\eta^5}\cos(\nu)\dot{\nu}nt & 0 & \sin(\lambda_\nu)\dot{\nu} & -\cos(\lambda_\nu)\dot{\nu} & 0 & 0 \\ -\frac{3}{2}\frac{e}{\eta^5}\sin(\nu)n & & & & & \\ -\frac{3}{2}\frac{\dot{\rho}}{\eta^3}nt - \frac{3}{2}\frac{\rho}{\eta^5}n & -\frac{1}{\rho^2}\dot{\rho} & \frac{-\frac{1}{\rho^2}\dot{\rho}\sin(\lambda_\nu)}{+(\frac{1}{\rho}+1)\cos(\lambda_\nu)\dot{\nu}} & \frac{-\frac{1}{\rho^2}\dot{\rho}\cos(\lambda_\nu)}{+(\frac{1}{\rho}+1)\sin(\lambda_\nu)\dot{\nu}} & 0 & 0 \\ 0 & 0 & 0 & 0 & \frac{-\frac{1}{\rho^2}\dot{\rho}\sin(\lambda_\nu)}{+\frac{1}{\rho}\cos(\lambda_\nu)\dot{\nu}} & \frac{\frac{1}{\rho^2}\dot{\rho}\cos(\lambda_\nu)}{+\frac{1}{\rho}\sin(\lambda_\nu)\dot{\nu}} \end{array}\right] \quad (21)$$

where $\nu = \nu(t)$, $\lambda_\nu = \omega + \nu(t)$, $\rho = 1 + e\cos(\nu(t))$, $\dot{\rho} = -e\sin(\nu)\dot{\nu}$, $\eta = \sqrt{1-e^2}$, $n = \sqrt{\mu/a^3}$, and μ is the main gravitation parameter. The IC used in this paper are linked to the quasi-nonsingular ROE through the first order map

$$\mathbf{c}_k \approx \boldsymbol{M}_{HCW}(\boldsymbol{\alpha}) \begin{bmatrix} 1 & 0 & 0 & 0 & 0 & 0 \\ \frac{3}{2}nt & 1 & 0 & 0 & 0 & 0 \\ 0 & 0 & 1 & 0 & 0 & 0 \\ 0 & 0 & 0 & 1 & 0 & 0 \\ 0 & 0 & 0 & 0 & 1 & 0 \\ 0 & 0 & 0 & 0 & 0 & 1 \end{bmatrix} \begin{pmatrix} (a_k - a)/a \\ (\omega_k + M_k(t) - \omega - M(t)) + (\Omega_k - \Omega)\cos(i) \\ e_k\cos(\omega_k) - e\cos(\omega) \\ e_k\sin(\omega_k) - e\sin(\omega) \\ i_k - i \\ (\Omega_k - \Omega)\sin(i) \end{pmatrix} \quad (22)$$

where

$$\boldsymbol{M}_{HCW}(\boldsymbol{\alpha}) = \begin{bmatrix} \eta^2 & 0 & 0 & 0 & 0 & 0 \\ 0 & \frac{1}{\eta} & -\left(\eta^2 - \frac{1}{\eta}\right)\frac{\sin(\omega)}{e} & \left(\eta^2 - \frac{1}{\eta}\right)\frac{\cos(\omega)}{e} & 0 & \left(\eta^2 - \frac{1}{\eta}\right)\cot(i) \\ 0 & \frac{e\sin(\omega)}{\eta} & \cos^2(\omega) + \frac{\sin^2(\omega)}{\eta} & \cos(\omega)\sin(\omega) - \frac{\cos(\omega)\sin(\omega)}{\eta} & 0 & -\frac{e\sin(\omega)\cot(i)}{\eta} \\ 0 & -\frac{e\cos(\omega)}{\eta} & \cos(\omega)\sin(\omega) - \frac{\cos(\omega)\sin(\omega)}{\eta} & \sin(\omega)^2 + \frac{\cos(\omega)^2}{\eta} & 0 & \frac{e\cos(\omega)\cot(i)}{\eta} \\ 0 & 0 & 0 & 0 & \eta^2 & 0 \\ 0 & 0 & 0 & 0 & 0 & \eta^2 \end{bmatrix} \quad (23)$$

and, in the ROE, $M(t)$ is the mean anomaly at instant t. The center matrix in Eq. 22 back-propagates the ROE to initial integration instant ($t = 0$) through the integrable dynamics. For $e \to 0$, $\boldsymbol{M}_{HCW}$ becomes identity (the singularities cancel out), and the IC used in this paper reduce to the quasi-nonsingular ROE and to the HCW's IC [19].

REFERENCES

[1] Jacklin, S. A., "Small-satellite mission failure rates", No. NASA/TM-2018-220034, 2019.

[2] Dezfuli, H., et al., "NASA Risk Management Handbook. Version 1.0", 2011.

[3] Woffinden, D. C., Geller, D. K., "Navigating the Road to Autonomous Orbital Rendezvous," *Journal of Spacecraft and Rockets*, Vol. 44, No. 4, 2007, pp. 898-909.

[4] Harting, A., et al., "On the collision hazard of colocated geostationary satellites", *AIAA/AAS Astrodynamics conference*, Minneapolis, 1988.

[5] D'Errico, M., *Distributed Space Missions for Earth System Monitoring*, Springer, New York, 2013.

[6] D'Amico, S., Montenbruck, O., "Proximity Operations of Formation-Flying Spacecraft Using an Eccentricity/Inclination Vector Separation", *Journal of Guidance, Control, and Dynamics*, Vol. 29, No. 3, 2006, pp. 554–563.

[7] Koenig A., D'Amico S., "Robust and Safe N-Spacecraft Swarming in Perturbed Near-Circular Orbits", *Journal of Guidance, Control, and Dynamics*, Vol. 41, No. 8, 2018, pp. 1643-1662.

[8] Guffanti, T., D'Amico, S., "Integration Constants as State Variables for Optimal Path Planning", *European Control Conference*, Lymassol, Cyprus, June 12-15, 2018.

[9] Guffanti T., D'Amico S., "Multi-Agent Passive Safe Optimal Control using Integration Constants as State Variables", *AIAA Scitech 2021 Forum*, Virtual Event, Jan. 11-15 & 19-21 (2021).

[10] Lakshmikantham, V., Deo, S.G., *Method of Variation of Parameters for Dynamic Systems*, Series in Mathematical Analysis and Applications, Vol. 1, Gordon and Breach Science, Amsterdam, 1998.

[11] Morgan, D., Chung, S.-J., Hadaegh, F. Y., "Model Predictive Control of Swarms of Spacecraft Using Sequential Convex Programming", *Journal of Guidance, Control, and Dynamics*, Vol. 37, No. 6, 2014, pp. 1725-1740.

[12] Bonalli, R., Cauligi, A., Bylard, A., Pavone, M., "GuSTO: Guaranteed sequential trajectory optimization via sequential convex programming", *In Proc. IEEE Conf. on Robotics and Automation*, Montreal, Canada, May 2019.

[13] Borrelli, F., Bemporad, A., Morari, M., *Predictive control for linear and hybrid systems*. Cambridge University Press, 2017.

[14] Koenig, A.W., D'Amico, S., Lightsey, E.G., "Formation Flying Orbit and Control Concept for the VISORS Mission", *AIAA Scitech 2021 Forum*, Nashville, Tennessee, Jan. 11-15 (2021).

[15] Vallado, D.A., *Fundamentals of Astrodynamics and Applications*, Space Technology Library, 2013.

[16] Casotto, S., "The equations of relative motion in the orbital reference frame", *Celest Mech Dyn Astr*, 124, 215–234 (2016).

[17] Clohessy, W.H., Wiltshire, R.S., "Terminal Guidance System for Satellite Rendezvous", *Journal of the Aerospace Sciences*, Vol. 27, No. 9, 1960, pp. 653–658.

[18] Yamanaka, K., Ankersen, F., "New State Transition Matrix for Relative Motion on an Arbitrary Elliptical Orbit", *Journal of Guidance, Control, and Dynamics*, Vol. 25, No. 1, 2002, pp. 60–66.

[19] D'Amico, S., "Relative Orbital Elements as Integration Constants of Hills Equations", DLR, TN (2005): 05-08.

[20] Boyd, S., Vandenberghe, L., *Convex Optimization*, Cambridge University Press, 2004.

[21] Domahidi, A., Chu, E., Boyd, S., "ECOS: An SOCP solver for embedded systems", *European Control Conference*, 2013, pp. 3071-3076.

[22] Giralo, V., *Precision Navigation of Miniaturized Distributed Space Systems using GNSS*, Ph.D. Thesis, Stanford University, 2021.

TABLE I

VISORS MISSION'S SWARM RECONFIGURATION SCENARIO [14].

Reference orbit		Relative orbit modes			Transfer & safety		Navigation [22]		Actuation [23]	
type	chief	type	Stand-by (t_0)	Science (t_f)	$t_f - t_0$ (orbits)	2	type	GPS	type	impulsive
a (km)	R_E + 500	ac_1 (m)	10	0	PS type	RN	*Unc.* ($1-\sigma$, per axis)		Min. imp. bit (Ns)	1e-3
e (-)	0.001	ac_2 (m)	-100	10	T (orbits)	2	Abs. position (m)	1	Min. imp. incr. (Ns)	6e-5
i (deg)	98	ac_3 (m)	0	25	ϵ (m)	3	Abs. velocity (cm/s)	1	*Unc.* ($1-\sigma$)	
Ω (deg)	252	ac_4 (m)	200	0	q (σ)	3	Rel. position (cm)	1	Maneuver magn. (%)	5
ω (deg)	0	ac_5 (m)	0	15	$\mathcal{J}$ (m/s)	$\sum_{ki} \|\|\tilde{\boldsymbol{u}}_k(t_i)\|\|_2$	Rel. velocity (μm/s)	25	Maneuver dir. (arcmin)	1
$\lambda_\nu(t_0)$ (deg)	-90	ac_6 (m)	200	0						
period (h)	1.58									
Epoch	1-1-2024									

TABLE II

SPACECRAFT FEATURES AND DYNAMICS MODELS.

Spacecraft features		Dynamics models		
Mass (kg)	12	type	Ground-truth [14], [22]	On-board [24], [25], [26]
Cross-section area (m^2)	nom: 0.285 avg: 0.206	Geopotential	GGM01S (60×60)	J_2 secular & long-period
		Atmospheric drag	NRLMSISE00	Secular & long-period model-free
C_d (-)	2.3	Solar radiation pressure	Cannonball model, no eclipses	Secular & long-period proportional to differential ballistic coefficients
C_r (-)	1.88	Third-body gravity	Analytical lunisolar ephemerides	Lunisolar secular & long-period
		Integrator	RK4	Euler
		Step size	Fixed: 30s	Fixed: period/12
		Process-noise on IC (m/orbit)	None	3

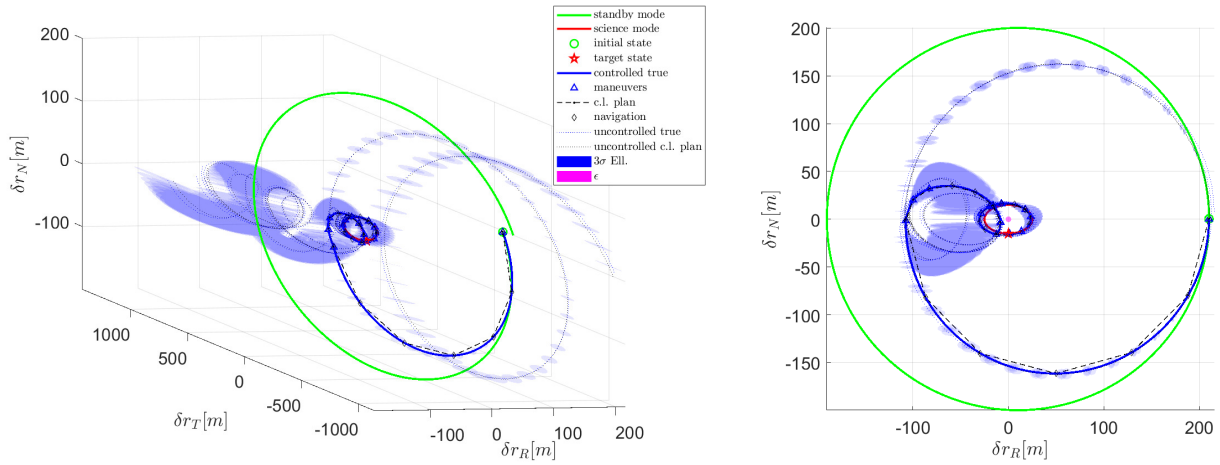

Fig. 6. Passively safe transfer trajectory in Cartesian RTN frame (3-D, left, and RN, right).

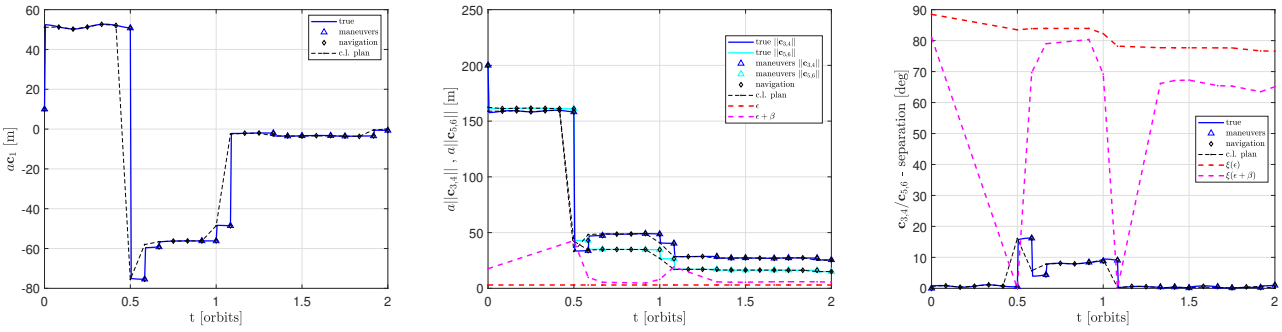

Fig. 7. IC trajectories and comparison with closed-form solutions.

[23] Lightsey, E.G., Stevenson, T., Sorgenfrei, M., "Development and Testing of a 3-D-Printed Cold Gas Thruster for an Interplanetary CubeSat", *Proceedings of the IEEE*, Vol. 106, No. 3, pp. 379–390, 2018.

[24] Koenig, A.W., Guffanti, T., D'Amico, S., "New State Transition Matrices for Spacecraft Relative Motion in Perturbed Orbits", *Journal of Guidance, Control, and Dynamics*, Vol. 40, No. 7, 2017, pp. 1749-1768.

[25] Guffanti, T., D'Amico, S., Lavagna, M., "Long-Term Analytical Propagation of Satellite Relative Motion in Perturbed Orbits", *AAS/AIAA Space Flight Mechanics Meeting*, San Antonio, Feb. 5-9, 2017.

[26] Guffanti, T., D'Amico, S., "Linear Models for Spacecraft Relative Motion Perturbed by Solar Radiation Pressure", *Journal of Guidance, Control, and Dynamics*, Vol. 42, No. 9, 2019, pp. 1962-1981.